Iğdır Üniversitesi Fen Bilimleri Enstitüsü Dergisi, 14(1), 209-218, 2024
Journal of the Institute of Science and Technology, 14(1), 209-218, 2024

ISSN: 2146-0574, eISSN: 2536-4618

Physics **DOI: 10.21597/jist.1376078**

Research Article

Received: 14.10.2023 **Accepted: 10.11.2023**

To Cite: Koç, F. (2024). Efficient Energy Level Calculations in InP 2D-Quantum Box with Two Distinct Potentials Using the Sparse Numerov Method. *Journal of the Institute of Science and Technology*, 14(1), 209-218.

Efficient Energy Level Calculations in InP 2D-Quantum Box with Two Distinct Potentials Using the Sparse Numerov Method

Fatih KOÇ

Highlights:

- The suitability of the sparse Numerov approach for 2D nanostructures is affirmed
- The sparse Numerov approach necessitates significantly fewer system resources compared to the classical Numerov method
- Efficient solution of power-exponential potential using sparse matrix method

ABSTRACT:

In this study, energy level calculations for an InP 2D quantum box structure with two distinct (infinite potential power-exponential) potential potentials have been conducted using the sparse Numerov method. The 2D Schrödinger equation has been transformed in accordance with the sparse Numerov approach, followed by the creation of the solution matrix employing appropriate finite difference expressions. A comparative analysis of calculation results has been performed with respect to CPU time, memory usage, and ground state energy for both $O(h^4)$ and $O(h^6)$ accuracy. The suitability of the sparse Numerov method for 2D nanostructures has been thoroughly discussed. The results revealed that the sparse Numerov approach yields physically meaningful and rational outcomes in the InP 2D quantum box structure. Importantly, it demands significantly lower CPU time and memory resources compared to the classical Numerov method, emphasizing its practical applicability in this context.

Keywords:

- Sparse Numerov approach
- 2D quantum box
- Nanostructure
- 2D-Stencil

Fatih KOÇ (**Orcid ID:** 0000-0002-4751-2340), Kırşehir Ahi Evran University, Faculty of Engineering and Architecture, Department of Metallurgical and Materials Engineering, Kırşehir, Türkiye

Corresponding Author: Fatih KOÇ, e-mail: fatih.koc@msn.com

INTRODUCTION

Semiconductor nanostructures (SCNSs) have emerged as versatile tools for various device applications owing to their size-dependent band gap energy, material-specific band alignment, enhanced quantum efficiency, and quantum coherency. These inherent characteristics enable SCNSs to meticulously tailor their optical and electronic properties, rendering them as promising candidates for a wide range of applications. These applications span diverse fields, including light-emitting diodes (LEDs) (Terada et al., 2022; Lu et al., 2023), lasers (Rafailov et al., 2007; Yadav et al., 2023), photovoltaic devices (Hu et al., 2021; Wang et al., 2023), quantum computation (Wang et al., 2022), and spintronics (Li et al., 2022). Given the extensive range of their utilities, SCNSs have attracted considerable attention from both theoretical and experimental researchers (Jiang et al, 2023; Ed-Dahmouny et al., 2023), particularly in recent years.

Solving the Schrödinger equation is an essential component of calculations involving the electronic and optical properties of SCNSs. The dimensionality of this equation (1D, 2D, or 3D) is contingent upon the geometry of the structure and the desired outcomes. Frequently, numerical methods prove to be the most suitable means to tackle this challenge. Within the scientific literature, numerous methods for solving the Schrödinger equation have been documented (Killingbeck, 1987; Koch et al., 2006; Gamper et al., 2023), with the choice of method contingent upon the specific characteristics of the nanostructure under investigation, each method harboring its own set of advantages and disadvantages. Notably, among these methods, the Numerov method emerges as a versatile solution capable of addressing the Schrödinger equation in 1D, 2D, and 3D dimensions (Kolagiratou et al., 2005; Graen & Grubmüller, 2016), thus providing more stable and reliable results.

The Numerov method, while versatile in its application to various nanostructures, comes with significant computational demands, particularly as the size of the nanostructure increases. This is especially pronounced in systems that require the solution of the Schrödinger equation in 2- or 3-dimensions. In such cases, the formation of large matrices for the eigenvalue problem becomes necessary, demanding high CPU power and memory resources, and consequently resulting in prolonged computation times. Additionally, it's important to note that the Numerov method has limitations in achieving a high degree of accuracy when solving the 2- and 3-dimensional Schrödinger equation (Graen & Grubmüller, 2016). This limitation can lead to a loss of computational precision, especially in specific geometries and specialized calculations.

On the other hand, while the Numerov method can achieve higher accuracy through a method recommended by Dongjiao (2014), Kuenzer et al. (2016) have taken the Numerov method to the next level, unveiling an approach that notably reduces CPU and memory usage, particularly in 2- and 3-dimensional Numerov solutions. This pioneering approach has been documented in the literature as the sparse Numerov approach. With the sparse Numerov approach, it becomes feasible to construct a sparse matrix, ensuring that the matrix needed for the eigenvalue problem remains symmetric. Consequently, substantial benefits have been realized in terms of both CPU and memory consumption. The sparse Numerov approach enables more efficient results, particularly in considerably larger systems or cases where the nanostructure problem demands a 2- or 3-dimensional Schrödinger equation solution.

In this study, the 2D Schrödinger equation has been solved fully numerically using the sparse Numerov approach to determine the energy levels of the 2D quantum box structure for two distinct potentials. The Schrödinger equation has been approximated with both $O(h^4)$ and $O(h^6)$ accuracy levels using their respective finite difference expressions. Additionally, sensitivity analyses has been carried out, and comparisons of CPU time and memory usage has been conducted.

MATERIALS AND METHODS

In this study, a 2D InP quantum box structure has been chosen as the model structure, and full numerical calculations have been performed using different potential profiles. The governing equation for this system is the 2D Schrödinger equation, which is expressed as:

$$-\frac{\hbar^2}{2m}\left(\frac{\partial^2\psi(x,y)}{\partial x^2}+\frac{\partial^2\psi(x,y)}{\partial y^2}\right)+V(x,y)\psi(x,y)=E\psi(x,y). \quad (1)$$

During the numerical solution of the 2D Schrödinger equation, the Numerov method has been utilized as the preferred computational technique. This method is well-known for its adaptability, as it can be applied to solve all ordinary differential equations expressed in the form $\Delta\psi(x,y)=f(x,y)\psi(x,y)$. To make the Schrödinger equation compatible with the Numerov method, it can be rearranged as:

$$\Delta\psi\,(x,y\,)=\frac{2m}{\hbar^2}(V(\,x,y)\,-E)\,\psi(x,y)=f(x,y)\psi(x,y) \quad (2)$$

where $V(x,y)$ is the 2D confinement potential, E is the energy eigenvalue, and $\psi(x,y)$ signifies the wavefunction of the system. With the utilization of the standard Numerov method, the energy eigenvalues and wave functions of a quantum system can be expressed as (Pillai et al., 2012):

$$\mathbb{A}\psi+\mathbb{B}\mathbb{V}\psi=E\psi\Longrightarrow(\mathbb{B}^{-1}\mathbb{A}+\mathbb{V})\psi=E\psi. \quad (3)$$

It's important to highlight that $\mathbb{A}$ and $\mathbb{B}$ represent tridiagonal, symmetric, and sparse matrices; however, products like $\mathbb{B}^{-1}\mathbb{A}$ are generally not symmetric. When dealing with eigenvalue problems for matrices of types $\mathbb{A}$ and $\mathbb{B}$, the utilization of specialized sparse matrix algorithms available in libraries such as Armadillo (Sanderson & Curtin, 2016; Sanderson & Curtin, 2018) significantly enhances efficiency and reduces system resource requirements. However, for multiplications like $\mathbb{B}^{-1}\mathbb{A}$ in general, the need to resort to a dense matrix solution becomes unavoidable. This leads to a substantial increase in computation time, memory usage, and CPU consumption, particularly when addressing the 2D Schrödinger equation using the standard Numerov method. These demands become increasingly evident as the size of the structure being studied grows. It's worth emphasizing that the standard Numerov method is limited in terms of accuracy, typically reaching only $O(h^4)$ accuracy. This limitation can considerably impact the overall precision of calculations, especially when applied to the 2D Schrödinger equation.

To address the accuracy limitations of the standard Numerov method, the literature contains studies that propose the use of the Numerov method with higher accuracy, as initially suggested by Dongjiao (2014), and subsequently adapted for the 2D and 3D Schrödinger equations by Kuenzer et al. (2016). The general form of the modified Numerov method applied with enhanced accuracy in two dimensions can be derived as follows:

$$\psi_{i+1,j+1}+\psi_{i+1,j-1}+\psi_{i-1,j+1}+\psi_{i-1,j-1}-4\psi_{i,j}=2h^2f_{i,j}\psi_{i,j}+$$
$$4\sum_{k=2}^{n}\frac{h^{2k}}{(2k)!}\left(\sum_{l=0}^{k}\frac{(2k)!}{(2k-2l)!(2l)!}\frac{\partial^{2k}\psi}{\partial x^{2k-2l}\partial y^{2l}}\right)+O(h^{2n+2}). \quad (4)$$

As illustrated by this equation, it's clear that accuracy can be tailored to the desired degree by adjusting the value of n. However, it's important to note that increasing n to achieve higher accuracy also results in a greater number of diagonals in the matrix that needs to be solved. Consequently, this leads to an increase in processing time and greater system resource requirements. Therefore, considering

these requirements, it is a more practical approach to determine an optimal value for n rather than pursuing extremely high accuracy.

In this study, calculations were conducted with $O(h^6)$ accuracy by selecting $n = 3$. When $n = 3$ is chosen, Equation 4. transforms into the following forms:

$$2f_{i,j}\psi_{i,j} = \frac{\psi_{i+1,j+1}+\psi_{i+1,j-1}+\psi_{i-1,j+1}+\psi_{i-1,j-1}-4\psi_{i,j}}{h^2} - \frac{4h^2}{4!}\left(\frac{\partial^4\psi}{\partial x^4} + 6\frac{\partial^4\psi}{\partial x^2\partial y^2} + \frac{\partial^4\psi}{\partial y^4}\right) - \frac{4h^4}{6!}\left(\frac{\partial^6\psi}{\partial x^6} + 15\frac{\partial^6\psi}{\partial x^4\partial y^2} + 15\frac{\partial^6\psi}{\partial x^2\partial y^4} + \frac{\partial^6\psi}{\partial y^6}\right) + O(h^6). \quad (5)$$

The issue of generally needing a dense matrix solution for the multiplication of matrices $\mathbb{B}^{-1}\mathbb{A}$ can be resolved by implementing the sparse Numerov method (Kuenzer et al., 2016). When the sparse Numerov method is employed, the eigenvalue equation takes the following form(Pillai et al., 2012):

$$(\mathbb{A} + \mathbb{V})\psi = \mathbb{H}\psi = E\psi \quad (6)$$

Here, matrices $\mathbb{A}$ and $\mathbb{V}$ possess the characteristics of being symmetric and sparse matrices, leading to matrix $\mathbb{H}$ also acquiring symmetry and sparsity. Only the main diagonal of the potential matrix $\mathbb{V}$ contains non-zero values, while all other entries are zeros. As a result, it exclusively influences only the main diagonal of the solution matrix in its entirety, preserving its symmetry. As previously mentioned, solving this eigenvalue problem becomes significantly faster and requires fewer system resources when utilizing specialized sparse matrix algorithms.

Taking into account all the provided information, the initial step involves applying finite difference expressions to Equation 5., which subsequently leads to the generation of the necessary matrix, $\mathbb{A}$, for the solution. As indicated by Equation 5., the expansion of fourth derivatives with $O(h^4)$ accuracy and sixth derivatives with $O(h^2)$ accuracy leads to the overall equation possessing $O(h^6)$ accuracy. Upon expanding all derivatives using finite difference methods and aggregating their contributions, the resulting 2D-stencil is as follows:

$$\begin{pmatrix} 0 & 0 & 0 & 0 & 0 & 0 & 0 \\ 0 & 0 & 0 & 0 & 0 & 0 & 0 \\ 0 & 0 & 0 & 0 & 0 & 0 & 0 \\ 0 & 0 & 0 & f_{i,j} & 0 & 0 & 0 \\ 0 & 0 & 0 & 0 & 0 & 0 & 0 \\ 0 & 0 & 0 & 0 & 0 & 0 & 0 \\ 0 & 0 & 0 & 0 & 0 & 0 & 0 \end{pmatrix} = \frac{1}{2h^2}\begin{pmatrix} 0 & 0 & 0 & \frac{1}{45} & 0 & 0 & 0 \\ 0 & -\frac{1}{144} & \frac{1}{36} & -\frac{41}{120} & \frac{1}{36} & -\frac{1}{144} & 0 \\ 0 & \frac{1}{36} & -\frac{1}{9} & \frac{19}{6} & -\frac{1}{9} & \frac{1}{36} & 0 \\ \frac{1}{45} & -\frac{41}{120} & \frac{19}{6} & -\frac{401}{36} & \frac{19}{6} & -\frac{41}{120} & \frac{1}{45} \\ 0 & \frac{1}{36} & -\frac{1}{9} & \frac{19}{6} & -\frac{1}{9} & \frac{1}{36} & 0 \\ 0 & -\frac{1}{144} & \frac{1}{36} & -\frac{41}{120} & \frac{1}{36} & -\frac{1}{144} & 0 \\ 0 & 0 & 0 & \frac{1}{45} & 0 & 0 & 0 \end{pmatrix} \quad (7)$$

The right side of Equation 7. represents the main matrix necessary for solving the 2D Schrödinger equation. Within each row or column of the stencil lies the diagonals of distinct block matrices, collectively forming the main matrix. When considering symmetric matrices as one, it becomes evident that four distinct block matrices must be constructed to compose the main matrix. For instance if the problem is presumed to be resolved on an $M \times N$ grid, it is imperative to establish four distinct block matrices, each of $M \times N$ dimensions. As an example for a 10×10 grid problem, the block matrices established are as follows:

$$A=\begin{pmatrix} -\frac{401}{36} & \frac{19}{6} & -\frac{41}{120} & \frac{1}{45} & 0 & 0 & 0 & 0 & 0 & 0 \\ \frac{19}{6} & -\frac{401}{36} & \frac{19}{6} & -\frac{41}{120} & \frac{1}{45} & 0 & 0 & 0 & 0 & 0 \\ -\frac{41}{120} & \frac{19}{6} & -\frac{401}{36} & \frac{19}{6} & -\frac{41}{120} & \frac{1}{45} & 0 & 0 & 0 & 0 \\ \frac{1}{45} & -\frac{41}{120} & \frac{19}{6} & -\frac{401}{36} & \frac{19}{6} & -\frac{41}{120} & \frac{1}{45} & 0 & 0 & 0 \\ 0 & \frac{1}{45} & -\frac{41}{120} & \frac{19}{6} & -\frac{401}{36} & \frac{19}{6} & -\frac{41}{120} & \frac{1}{45} & 0 & 0 \\ 0 & 0 & \frac{1}{45} & -\frac{41}{120} & \frac{19}{6} & -\frac{401}{36} & \frac{19}{6} & -\frac{41}{120} & \frac{1}{45} & 0 \\ 0 & 0 & 0 & \frac{1}{45} & -\frac{41}{120} & \frac{19}{6} & -\frac{401}{36} & \frac{19}{6} & -\frac{41}{120} & \frac{1}{45} \\ 0 & 0 & 0 & 0 & \frac{1}{45} & -\frac{41}{120} & \frac{19}{6} & -\frac{401}{36} & \frac{19}{6} & -\frac{41}{120} \\ 0 & 0 & 0 & 0 & 0 & \frac{1}{45} & -\frac{41}{120} & \frac{19}{6} & -\frac{401}{36} & \frac{19}{6} \\ 0 & 0 & 0 & 0 & 0 & 0 & \frac{1}{45} & -\frac{41}{120} & \frac{19}{6} & -\frac{401}{36} \end{pmatrix}$$

$$B=\begin{pmatrix} \frac{19}{6} & -\frac{1}{9} & \frac{1}{36} & 0 & 0 & 0 & 0 & 0 & 0 & 0 \\ -\frac{1}{9} & \frac{19}{6} & -\frac{1}{9} & \frac{1}{36} & 0 & 0 & 0 & 0 & 0 & 0 \\ \frac{1}{36} & -\frac{1}{9} & \frac{19}{6} & -\frac{1}{9} & \frac{1}{36} & 0 & 0 & 0 & 0 & 0 \\ 0 & \frac{1}{36} & -\frac{1}{9} & \frac{19}{6} & -\frac{1}{9} & \frac{1}{36} & 0 & 0 & 0 & 0 \\ 0 & 0 & \frac{1}{36} & -\frac{1}{9} & \frac{19}{6} & -\frac{1}{9} & \frac{1}{36} & 0 & 0 & 0 \\ 0 & 0 & 0 & \frac{1}{36} & -\frac{1}{9} & \frac{19}{6} & -\frac{1}{9} & \frac{1}{36} & 0 & 0 \\ 0 & 0 & 0 & 0 & \frac{1}{36} & -\frac{1}{9} & \frac{19}{6} & -\frac{1}{9} & \frac{1}{36} & 0 \\ 0 & 0 & 0 & 0 & 0 & \frac{1}{36} & -\frac{1}{9} & \frac{19}{6} & -\frac{1}{9} & \frac{1}{36} \\ 0 & 0 & 0 & 0 & 0 & 0 & \frac{1}{36} & -\frac{1}{9} & \frac{19}{6} & -\frac{1}{9} \\ 0 & 0 & 0 & 0 & 0 & 0 & 0 & \frac{1}{36} & -\frac{1}{9} & \frac{19}{6} \end{pmatrix}$$

$$C=\begin{pmatrix} -\frac{41}{120} & \frac{1}{36} & -\frac{1}{144} & 0 & 0 & 0 & 0 & 0 & 0 & 0 \\ \frac{1}{36} & -\frac{41}{120} & \frac{1}{36} & -\frac{1}{144} & 0 & 0 & 0 & 0 & 0 & 0 \\ -\frac{1}{144} & \frac{1}{36} & -\frac{41}{120} & \frac{1}{36} & -\frac{1}{144} & 0 & 0 & 0 & 0 & 0 \\ 0 & -\frac{1}{144} & \frac{1}{36} & -\frac{41}{120} & \frac{1}{36} & -\frac{1}{144} & 0 & 0 & 0 & 0 \\ 0 & 0 & -\frac{1}{144} & \frac{1}{36} & -\frac{41}{120} & \frac{1}{36} & -\frac{1}{144} & 0 & 0 & 0 \\ 0 & 0 & 0 & -\frac{1}{144} & \frac{1}{36} & -\frac{41}{120} & \frac{1}{36} & -\frac{1}{144} & 0 & 0 \\ 0 & 0 & 0 & 0 & -\frac{1}{144} & \frac{1}{36} & -\frac{41}{120} & \frac{1}{36} & -\frac{1}{144} & 0 \\ 0 & 0 & 0 & 0 & 0 & -\frac{1}{144} & \frac{1}{36} & -\frac{41}{120} & \frac{1}{36} & -\frac{1}{144} \\ 0 & 0 & 0 & 0 & 0 & 0 & -\frac{1}{144} & \frac{1}{36} & -\frac{41}{120} & \frac{1}{36} \\ 0 & 0 & 0 & 0 & 0 & 0 & 0 & -\frac{1}{144} & \frac{1}{36} & -\frac{41}{120} \end{pmatrix}$$

$$D=\begin{pmatrix} \frac{1}{45} & 0 & 0 & 0 & 0 & 0 & 0 & 0 & 0 & 0 \\ 0 & \frac{1}{45} & 0 & 0 & 0 & 0 & 0 & 0 & 0 & 0 \\ 0 & 0 & \frac{1}{45} & 0 & 0 & 0 & 0 & 0 & 0 & 0 \\ 0 & 0 & 0 & \frac{1}{45} & 0 & 0 & 0 & 0 & 0 & 0 \\ 0 & 0 & 0 & 0 & \frac{1}{45} & 0 & 0 & 0 & 0 & 0 \\ 0 & 0 & 0 & 0 & 0 & \frac{1}{45} & 0 & 0 & 0 & 0 \\ 0 & 0 & 0 & 0 & 0 & 0 & \frac{1}{45} & 0 & 0 & 0 \\ 0 & 0 & 0 & 0 & 0 & 0 & 0 & \frac{1}{45} & 0 & 0 \\ 0 & 0 & 0 & 0 & 0 & 0 & 0 & 0 & \frac{1}{45} & 0 \\ 0 & 0 & 0 & 0 & 0 & 0 & 0 & 0 & 0 & \frac{1}{45} \end{pmatrix}$$

Upon scrutinizing the resulting block matrices, it becomes apparent that each of them exhibits symmetry, with only the diagonals in proximity to the main diagonal being populated.

In the second step essential for solving the problem, these block matrices need to be amalgamated to form the main matrix. For an $M \times N$ grid, the size of the main matrix formed is $(M \times N) \times (M \times N)$. If each of the aforementioned block matrices is regarded as a diagonal of the main matrix, matrix A constitutes the main diagonal, matrix B constitutes the immediate upper and lower diagonals, and matrices C and D form the subsequent upper and lower diagonals. The schematic representation of the main matrix, constructed by adhering to these steps, is as follows:

$$\begin{pmatrix}
\begin{pmatrix}\times&\times&\times\\\times&\boldsymbol{A}&\times\\\times&\times&\times\end{pmatrix} & \begin{pmatrix}\times&\times&\times\\\times&\boldsymbol{B}&\times\\\times&\times&\times\end{pmatrix} & \begin{pmatrix}\times&\times&\times\\\times&\boldsymbol{C}&\times\\\times&\times&\times\end{pmatrix} & \begin{pmatrix}\times&\times&\times\\\times&\boldsymbol{D}&\times\\\times&\times&\times\end{pmatrix} & \begin{pmatrix}0&0&0\\0&\mathbf{0}&0\\0&0&0\end{pmatrix} & \begin{pmatrix}0&0&0\\0&\mathbf{0}&0\\0&0&0\end{pmatrix} & \begin{pmatrix}0&0&0\\0&\mathbf{0}&0\\0&0&0\end{pmatrix} \\
\begin{pmatrix}\times&\times&\times\\\times&\boldsymbol{B}&\times\\\times&\times&\times\end{pmatrix} & \begin{pmatrix}\times&\times&\times\\\times&\boldsymbol{A}&\times\\\times&\times&\times\end{pmatrix} & \begin{pmatrix}\times&\times&\times\\\times&\boldsymbol{B}&\times\\\times&\times&\times\end{pmatrix} & \begin{pmatrix}\times&\times&\times\\\times&\boldsymbol{C}&\times\\\times&\times&\times\end{pmatrix} & \begin{pmatrix}\times&\times&\times\\\times&\boldsymbol{D}&\times\\\times&\times&\times\end{pmatrix} & \begin{pmatrix}0&0&0\\0&\mathbf{0}&0\\0&0&0\end{pmatrix} & \begin{pmatrix}0&0&0\\0&\mathbf{0}&0\\0&0&0\end{pmatrix} \\
\begin{pmatrix}\times&\times&\times\\\times&\boldsymbol{C}&\times\\\times&\times&\times\end{pmatrix} & \begin{pmatrix}\times&\times&\times\\\times&\boldsymbol{B}&\times\\\times&\times&\times\end{pmatrix} & \begin{pmatrix}\times&\times&\times\\\times&\boldsymbol{A}&\times\\\times&\times&\times\end{pmatrix} & \begin{pmatrix}\times&\times&\times\\\times&\boldsymbol{B}&\times\\\times&\times&\times\end{pmatrix} & \begin{pmatrix}\times&\times&\times\\\times&\boldsymbol{C}&\times\\\times&\times&\times\end{pmatrix} & \begin{pmatrix}\times&\times&\times\\\times&\boldsymbol{D}&\times\\\times&\times&\times\end{pmatrix} & \begin{pmatrix}0&0&0\\0&\mathbf{0}&0\\0&0&0\end{pmatrix} \\
\begin{pmatrix}\times&\times&\times\\\times&\boldsymbol{D}&\times\\\times&\times&\times\end{pmatrix} & \begin{pmatrix}\times&\times&\times\\\times&C&\times\\\times&\times&\times\end{pmatrix} & \begin{pmatrix}\times&\times&\times\\\times&\boldsymbol{B}&\times\\\times&\times&\times\end{pmatrix} & \begin{pmatrix}\times&\times&\times\\\times&\boldsymbol{A}&\times\\\times&\times&\times\end{pmatrix} & \begin{pmatrix}\times&\times&\times\\\times&\boldsymbol{B}&\times\\\times&\times&\times\end{pmatrix} & \begin{pmatrix}\times&\times&\times\\\times&\boldsymbol{C}&\times\\\times&\times&\times\end{pmatrix} & \begin{pmatrix}\times&\times&\times\\\times&\boldsymbol{D}&\times\\\times&\times&\times\end{pmatrix} \\
\begin{pmatrix}0&0&0\\0&\mathbf{0}&0\\0&0&0\end{pmatrix} & \begin{pmatrix}\times&\times&\times\\\times&\boldsymbol{D}&\times\\\times&\times&\times\end{pmatrix} & \begin{pmatrix}\times&\times&\times\\\times&\boldsymbol{C}&\times\\\times&\times&\times\end{pmatrix} & \begin{pmatrix}\times&\times&\times\\\times&\boldsymbol{B}&\times\\\times&\times&\times\end{pmatrix} & \begin{pmatrix}\times&\times&\times\\\times&\boldsymbol{A}&\times\\\times&\times&\times\end{pmatrix} & \begin{pmatrix}\times&\times&\times\\\times&\boldsymbol{B}&\times\\\times&\times&\times\end{pmatrix} & \begin{pmatrix}\times&\times&\times\\\times&\boldsymbol{C}&\times\\\times&\times&\times\end{pmatrix} \\
\begin{pmatrix}0&0&0\\0&\mathbf{0}&0\\0&0&0\end{pmatrix} & \begin{pmatrix}0&0&0\\0&\mathbf{0}&0\\0&0&0\end{pmatrix} & \begin{pmatrix}\times&\times&\times\\\times&\boldsymbol{D}&\times\\\times&\times&\times\end{pmatrix} & \begin{pmatrix}\times&\times&\times\\\times&\boldsymbol{C}&\times\\\times&\times&\times\end{pmatrix} & \begin{pmatrix}\times&\times&\times\\\times&\boldsymbol{B}&\times\\\times&\times&\times\end{pmatrix} & \begin{pmatrix}\times&\times&\times\\\times&\boldsymbol{A}&\times\\\times&\times&\times\end{pmatrix} & \begin{pmatrix}\times&\times&\times\\\times&\boldsymbol{B}&\times\\\times&\times&\times\end{pmatrix} \\
\begin{pmatrix}0&0&0\\0&\mathbf{0}&0\\0&0&0\end{pmatrix} & \begin{pmatrix}0&0&0\\0&\mathbf{0}&0\\0&0&0\end{pmatrix} & \begin{pmatrix}0&0&0\\0&\mathbf{0}&0\\0&0&0\end{pmatrix} & \begin{pmatrix}\times&\times&\times\\\times&\boldsymbol{D}&\times\\\times&\times&\times\end{pmatrix} & \begin{pmatrix}\times&\times&\times\\\times&\boldsymbol{C}&\times\\\times&\times&\times\end{pmatrix} & \begin{pmatrix}\times&\times&\times\\\times&\boldsymbol{B}&\times\\\times&\times&\times\end{pmatrix} & \begin{pmatrix}\times&\times&\times\\\times&\boldsymbol{A}&\times\\\times&\times&\times\end{pmatrix}
\end{pmatrix}$$

In the final step, the potential matrix $\mathbb{V}$, with dimensions $M \times N$ for the 2D Schrödinger equation, is generated and added to the matrix $\mathbb{A}$ to produce the matrix $\mathbb{H}$. By solving the eigenvalue problem for $\mathbb{H}$, the energy levels of the 2D system and their corresponding wave functions can be determined.

RESULTS AND DISCUSSION

In this study, InP has been considered as the material of the 2D quantum box, and eigenvalue solutions have been obtained using the sparse Numerov method. InP is characterized by high carrier mobility and low toxicity, making InP-based applications more reliable and promising as a future alternative to Cd-based applications (Zhang et al., 2019; Chen et al., 2020). In addition, with its large absorption coefficient and tunable emission from the visible to the near-infrared region, different nano-sized InP quantum structures (dot/wire/disk) can be used in many areas such as quantum LEDs (Won et al., 2019), quantum dot/dash lasers (Liu et al., 2023), quantum sensing applications (Chang et al., 2023) and etc (Liang et al., 2022).

Throughout the calculations, atomic units have been employed, where fundamental constants such as charge, bare mass, and Planck's constant have all been set to unity, i.e., $e = m_0 = \hbar = 1$, for simplicity. In these atomic units, with InP as the reference material, the atomic Bohr radius of the structure has been determined as $1a_0 \cong 82.7$ Å , and the effective Rydberg energy has been found to be $1Ry \cong 7.0\ meV$. The effective mass of the electron in InP has been taken as $0.08\ m_0$. The step size used in the calculations has been set to 0.01. To clarify, when referring to a 100×100 grid, it indicates that the structure spans dimensions of $1a_0$ in both the *x* and *y* directions.

The initial step involved the calculation of energy levels for a structure with an infinite potential, as described in Equation 8. The primary objective was to assess the variance in precision between computations conducted at accuracy levels of $O(h^4)$ and $O(h^6)$. Calculating with infinite potential has been chosen because it offers a more straightforward analysis of energy levels and has provided reliable data for comparing numerical results.

$$V(x,y) = \begin{cases} 0, & x,y < x_{max}, y_{max} \\ \infty, & x,y \geq x_{max}, y_{max} \end{cases} \tag{8}$$

In Table 1., the calculation results for the 2D InP quantum box with infinite potential are presented. The table includes CPU time, memory utilization by the main matrix, and ground state energies for both $O(h^4)$ and $O(h^6)$ accuracy levels, categorized by various grid sizes. The last column of the table provides analytical calculation results for the ground state energy levels of a structure with the same grid dimensions. As observed in the table, there is a noticeable difference in ground state energy levels between $O(h^4)$ and $O(h^6)$ accuracy levels in small grid sizes. Additionally, these energy levels, calculated with the sparse Numerov method, appear to deviate somewhat from the analytical values at small grid sizes. However, as the grid sizes increase, the difference in energy levels $O(h^4)$ and $O(h^6)$ accuracy decreases significantly. They gradually converge to each other and to the analytical values.

Table 1. Comparison of the CPU times, matrices sizes and ground state energy levels

	$O(h^4)$			$O(h^6)$			
N Grid	**CPU Time (s)**	**M. Size (kbytes)**	**GS Energy (meV)**	**CPU Time (s)**	**M. Size (kbytes)**	**GS Energy (meV)**	**R. Energy (meV)**
50 × 50	2.24	175.23	527.98	5.36	551.49	532.25	550.02
100 × 100	16.35	710.43	134.68	70.33	2262.69	135.21	137.51
150 × 150	53.24	1605.63	60.26	259.98	5133.89	60.42	61.11
200 × 200	164.63	2860.83	34.01	690.17	9165.09	34.08	34.38
250 × 250	426.45	4476.03	21.81	1634.31	14356.30	21.84	22.00
300 × 300	900.56	6451.23	15.17	3378.67	20707.50	15.19	15.28
350 × 350	1670.92	8786.43	11.15	5475.33	28218.70	11.17	11.22
400 × 400	2392.66	11481.60	8.55	8875.11	36889.90	8.55	8.59

On the other hand, in terms of CPU time comparisons, it becomes evident that calculations performed with $O(h^6)$ accuracy demand roughly four times more CPU time compared to calculations conducted with $O(h^4)$ accuracy. Moreover, as the grid size increases, CPU time exhibits a rapid increase. A similar pattern is observed in the memory usage attributed to the main matrix established for eigenvalue calculations. Specifically, calculations executed with $O(h^6)$ accuracy result in approximately 3.2 times more memory consumption compared to those performed with $O(h^4)$ accuracy. Based on these findings, it can be concluded that achieving $O(h^6)$ accuracy in ground state energy level calculations may not be necessary, particularly when dealing with larger structures, as it entails increased CPU time and memory usage.

In this study, power-exponential potential as described in Equation 9. (Ciurla et al., 2002) has been employed. Calculations have been performed using this 2D potential, considering different grid sizes and k parameters with $O(h^6)$ accuracy, and the results have been subsequently compared and analyzed.

$$V(r) = V_0 * (1 - e^{(-r/R_{max})k}). \quad (9)$$

Here, a bare InP quantum box is considered and the effect of the power-exponential potential on the energy levels at higher values of k is observed. To facilitate this investigation, V_0 has been set at $2.72\ eV$. R_{max} has been defined as the edge length of the 2D quantum box, and r being determined as $r = \sqrt{x^2 + y^2}$.

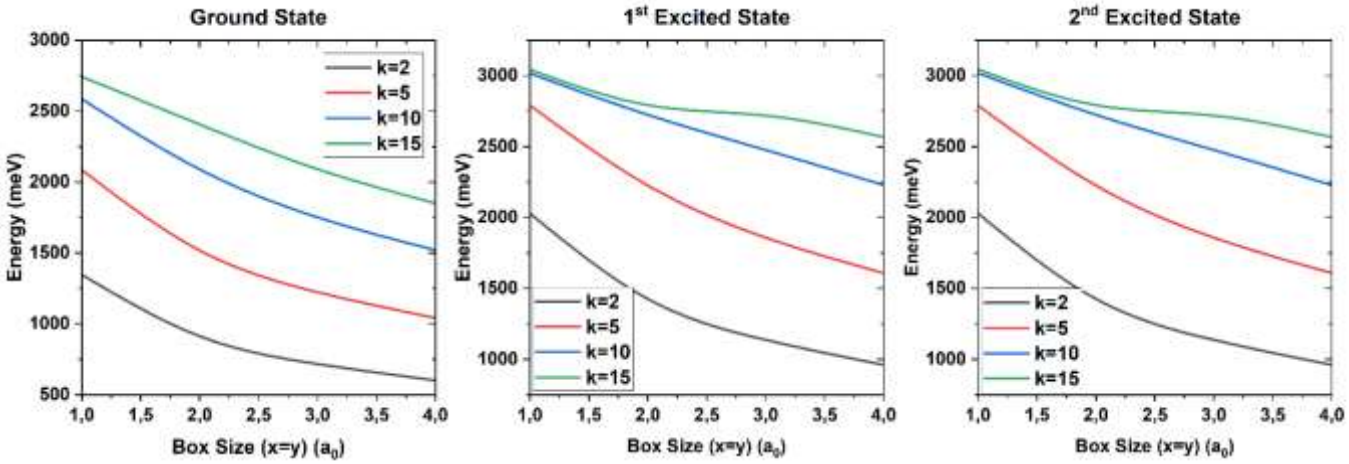

Figure 1. The ground state, 1^{st} excited state and 2^{nd} excited state energies of the 2D Quantum Box are presented as a function of the side length of the box for various values of the parameter k. These calculations were conducted with the assumption that the side lengths in both the x and y directions are equal ($x = y$)

Figure 1. illustrates the variation in energy levels for the ground state, 1^{st} excited state, and 2^{nd} excited state of the 2D quantum box as a function of the box size for different values of the parameter k. As expected, an increase in the size of the 2D box leads to a decrease in all energy levels. Furthermore, the figure clearly demonstrates that as the value of k increases, the energy levels also increase. According to Equation 9., this behavior can be attributed to the fact that with an increase in k, the potential V reaches its maximum, V_0 over a much shorter distance. Consequently, the confinement well, where the electron is localized, becomes narrower, resulting in an increase in energy levels. Figure 2. provides a visual representation of the potential changes with respect to varying values of k.

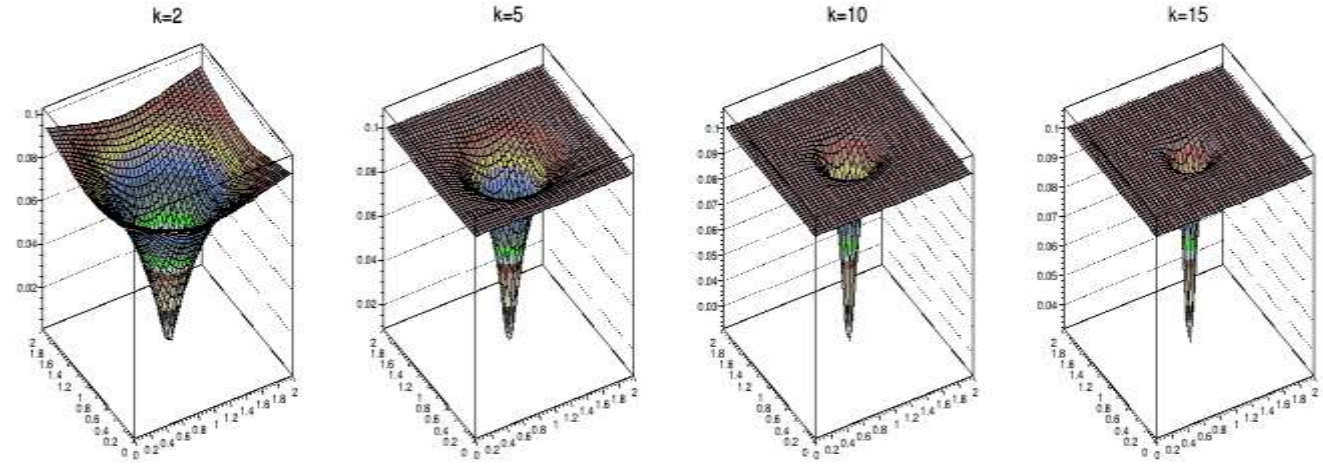

Figure 2. Schematic illustration depicting the variation in potential concerning the parameter k

Another noteworthy observation in Figure 1. is that, with increasing k, especially in smaller box sizes, the energy levels surpass the V_0 limiting potential, transitioning to free-state energy levels. This transition occurred for ground state energies only at $k = 15$ when the box dimensions were $1a_0 \times 1a_0$, as clearly depicted in the graph. For the 1^{st} and 2^{nd} excited states, which are degenerate as expected in the 2D box, such transitions are more common, given that these energy levels are higher than the ground state. As illustrated in Figure 1., the V_0 potential was exceeded at $k = 5, 10, 15$ in the $1a_0 \times 1a_0$ box dimensions, and at $k = 15$ in the $2a_0 \times 2a_0$box dimensions. The k parameter for this potential can be considered an effective tool for manipulating energy levels and controlling confinement in the system.

CONCLUSION

In conclusion, the results demonstrate that the sparse Numerov method provides sound and valid results for both potentials, thus confirming its applicability to 2D quantum nanostructures. This approach streamlines the analysis of larger structures by maintaining symmetry and facilitating sparse matrix solutions, consequently reducing the considerable burden on CPU and memory resources. However, it's crucial to note the observed deviation in energy levels, particularly noticeable in calculations involving small-sized structures with infinite potential. It appears that achieving higher accuracy levels is necessary for low-dimensional nanostructures in terms of computational precision.

REFERENCES

Chang, J., Gao, J., Esmaeil Zadeh, I., Elshaari, A. W., & Zwiller, V. (2023). Nanowire-based integrated photonics for quantum information and quantum sensing. *Nanophotonics*, 12(3), 339-358.

Chen, B., Li, D., & Wang, F. (2020). InP quantum dots: synthesis and lighting applications. *Small*, 16(32), 2002454.

Ciurla, M., Adamowski, J., Szafran, B., & Bednarek, S. (2002). Modelling of confinement potentials in quantum dots. *Physica E: Low-dimensional Systems and Nanostructures*, 15(4), 261-268.

Dongjiao, T., Ye, Y., & Dewanto, M. A. (2014). Generalized Matrix Numerov Solutions to the Schrödinger Equation. *Bachelorâ€™s thesis, National University of Singapore, Singapore*.

Ed-Dahmouny, A., Zeiri, N., Fakkahi, A., Arraoui, R., Jaouane, M., Sali, A., ... & Duque, C. A. (2023). Impurity photo-ionization cross section and stark shift of ground and two low-lying excited electron-states in a core/shell ellipsoidal quantum dot. *Chemical Physics Letters*, *812*, 140251.

Gamper, J., Kluibenschedl, F., Weiss, A. K., & Hofer, T. S. (2023). Accessing Position Space Wave Functions in Band Structure Calculations of Periodic Systems─ A Generalized, Adapted Numerov Implementation for One-, Two-, and Three-Dimensional Quantum Problems. *The Journal of Physical Chemistry Letters*, *14*(33), 7395-7403.

Graen, T., & Grubmüller, H. (2016). NuSol—Numerical solver for the 3D stationary nuclear Schrödinger equation. *Computer Physics Communications*, *198*, 169-178.

Hu, L., & Mandelis, A. (2021). Advanced characterization methods of carrier transport in quantum dot photovoltaic solar cells. *Journal of Applied Physics*, *129*(9).

Jiang, W., Low, B. Q. L., Long, R., Low, J., Loh, H., Tang, K. Y., ... & Ye, E. (2023). Active site engineering on plasmonic nanostructures for efficient photocatalysis. *ACS nano*, *17*(5), 4193-4229.

Killingbeck, J. (1987). Shooting methods for the Schrodinger equation. *Journal of Physics A: Mathematical and General*, *20*(6), 1411.

Kuenzer, U., Sorarù, J. A., & Hofer, T. S. (2016). Pushing the limit for the grid-based treatment of Schrödinger's equation: a sparse Numerov approach for one, two and three dimensional quantum problems. *Physical Chemistry Chemical Physics*, *18*(46), 31521-31533.

Koch, O., Kreuzer, W., & Scrinzi, A. (2006). Approximation of the time-dependent electronic Schrödinger equation by MCTDHF. *Applied mathematics and computation*, *173*(2), 960-976.

Li, J., Liu, X., Wan, L., Qin, X., Hu, W., & Yang, J. (2022). Mixed magnetic edge states in graphene quantum dots. *Multifunctional Materials*, *5*(1), 014001.

Liang, K., Wang, R., Huo, B., Ren, H., Li, D., Wang, Y., ... & Zhu, B. (2022). Fully printed optoelectronic synaptic transistors based on quantum dot–metal oxide semiconductor heterojunctions. *ACS nano*, 16(6), 8651-8661.

Liu, G., Poole, P. J., Lu, Z., Liu, J., Song, C. Y., Mao, Y., & Barrios, P. (2023). Mode-Locking and Noise Characteristics of InAs/InP Quantum Dash/Dot Lasers. *Journal of Lightwave Technology*, 41(13), 4262-4270.

Lu, P., Lu, M., Zhang, F., Qin, F., Sun, S., Zhang, Y., ... & Bai, X. (2023). Bright and spectrally stable pure-red CsPb (Br/I) 3 quantum dot LEDs realized by synchronous device structure and ligand engineering. *Nano Energy*, *108*, 108208.

Pillai, M., Goglio, J., & Walker, T. G. (2012). Matrix Numerov method for solving Schrödinger's equation. *American Journal of Physics*, *80*(11), 1017-1019.

Rafailov, E. U., Cataluna, M. A., & Sibbett, W. (2007). Mode-locked quantum-dot lasers. *Nature photonics*, *1*(7), 395-401.

Sanderson, C., & Curtin, R. (2016). Armadillo: a template-based C++ library for linear algebra. *Journal of Open Source Software*, *1*(2), 26.

Sanderson, C., & Curtin, R. (2018). A user-friendly hybrid sparse matrix class in C++. In *Mathematical Software–ICMS 2018: 6th International Conference, South Bend, IN, USA, July 24-27, 2018, Proceedings 6* (pp. 422-430). Springer International Publishing.

Terada, S., Ueda, H., Ono, T., & Saitow, K. I. (2022). Orange–red Si quantum dot LEDs from recycled rice husks. *ACS Sustainable Chemistry & Engineering*, *10*(5), 1765-1776.

Wang, K., Xu, G., Gao, F., Liu, H., Ma, R. L., Zhang, X., ... & Guo, G. P. (2022). Ultrafast coherent control of a hole spin qubit in a germanium quantum dot. *Nature Communications*, *13*(1), 206.

Wang, X., Xu, L., Ge, S., Foong, S. Y., Liew, R. K., Chong, W. W. F., ... & Huang, R. (2023). Biomass-based carbon quantum dots for polycrystalline silicon solar cells with enhanced photovoltaic performance. *Energy*, *274*, 127354.

Won, Y. H., Cho, O., Kim, T., Chung, D. Y., Kim, T., Chung, H., ... & Jang, E. (2019). Highly efficient and stable InP/ZnSe/ZnS quantum dot light-emitting diodes. *Nature*, 575(7784), 634-638.

Yadav, A., Chichkov, N. B., Avrutin, E. A., Gorodetsky, A., & Rafailov, E. U. (2023). Edge emitting mode-locked quantum dot lasers. *Progress in Quantum Electronics*, 100451.

Zhang, H., Hu, N., Zeng, Z., Lin, Q., Zhang, F., Tang, A., ... & Du, Z. (2019). High-efficiency green InP quantum dot-based electroluminescent device comprising thick-shell quantum dots. *Advanced Optical Materials*, 7(7), 1801602.